Time-resolved and time-scale adaptive measures of spike train synchrony

Thomas Kreuz [a,*], Daniel Chicharro [b], Martin Greschner [c], Ralph G. Andrzejak [b],

[a] Institute for Complex Systems, CNR, Sesto Fiorentino, Italy
[b] Department of Information and Communication Technologies, Universitat Pompeu Fabra, Barcelona, Spain
[c] The Salk Institute for Biological Studies, San Diego, California, USA

Abstract

A wide variety of approaches to estimate the degree of synchrony between two or more spike trains have been proposed. One of the most recent methods is the ISI-distance which extracts information from the interspike intervals (ISIs) by evaluating the ratio of the instantaneous firing rates. In contrast to most previously proposed measures it is parameter free and time-scale independent. However, it is not well suited to track changes in synchrony that are based on spike coincidences. Here we propose the SPIKE-distance, a complementary measure which is sensitive to spike coincidences but still shares the fundamental advantages of the ISI-distance. In particular, it is easy to visualize in a time-resolved manner and can be extended to a method that is also applicable to larger sets of spike trains. We show the merit of the SPIKE-distance using both simulated and real data.

1. Introduction

In recent years measures of multi-neuron synchrony have become indispensable tools in order to address issues such as network synchronization and population coding. In this context, measures that are sensitive to spike coincidences are not only of theoretical importance but also of high practical relevance, since coincidences of spikes have been proven to be of high prevalence in many different neuronal circuits. Examples include olfactory bulb (Wilson and Mainen, 2006), hippocampus (Best et al., 2001), somatosensory cortex (Romo and Salinas, 2003), auditory cortex (Schreiner et al., 2007), visual cortex (Usrey et al., 1999; Priebe and Ferster, 2008), and retina (Meister and Berry, 1995; Field and Chichilnisky, 2007). In all these systems the firing of different neurons has been shown to be correlated.

A wide variety of approaches to quantify the dissimilarity, or distance, between two spike trains has been proposed. Most widely used is the metric introduced in Victor and Purpura (1996) which evaluates the cost needed to transform one spike train into the other using only certain elementary steps. This method involves one parameter that sets the time-scale. In contrast, a more recent approach, the ISI-distance, is parameter free and time-scale adaptive (Kreuz et al., 2007). On spike trains extracted from a simulated Hindemarsh-Rose network the ISI-distance could re-

produce a known clustering equally well as the best time-scale-optimized measure (Kreuz et al., 2007). Recently, two multiple spike train extensions of the ISI-distance have been proposed, the local pairwise average and a multivariate measure based on the coefficient of variation (Kreuz et al., 2009).

The ISI-distance and its extensions are based on the relative length of simultaneous interspike intervals (ISI) and are thus well-designed to quantify similarities in the neurons' firing rate profiles. However, they are not optimally suited to track the type of synchrony which is mediated by changes in the fraction of coincident spikes. In this study we propose the SPIKE-distance, a measure which inherits the advantages of the ISI-distance, but shifts the focus of attention from the interspike intervals to the timing of the spikes. Given two spike trains, for each time instant the absolute differences between the previous spike times and the following spike times are averaged and normalized by the mean length of the interspike intervals. Furthermore, also for the SPIKE-distance we propose two extensions to the case of multiple spike trains, either as a local pairwise average or as a multivariate measure.

We use several sets of specifically designed and simulated spike trains in order to illustrate the properties of the SPIKE-distance and compare its performance to the one of previously published methods such as the ISI-distance, the Victor-Purpura distance and the correlation coefficient. In a first application to real data we employ the spiking activity of a population of retinal ganglion cells (Meister and Berry, 1995; Field and Chichilnisky, 2007) as an ideal

---

* Corresponding author.
  Email address: `thomas.kreuz@cnr.it` (Thomas Kreuz).

testing ground for the different measures. In particular, we evaluate their capability to reproduce the gradual decrease of synchrony between two retinal ganglion cells with the distance between their receptive fields (Meister et al., 1995; Shlens et al., 2006). As a second application to real data we employ the spike train distances to discriminate single-unit responses to taste stimuli recorded in the nucleus of the solitary tract (NTS) in rats (Di Lorenzo and Victor, 2003; data available online at http://neurodatabase.org/, Gardner, 2004). In this case the performance of the various measures is quantified by the normalized mutual information of the confusion matrix (Abramson, 1963; Victor and Purpura, 1996).

The remainder of the paper is organized as follows: In Section 2.1 we describe the new SPIKE-distance and its extensions. Subsequently, we use constructed examples to stress the different sensitivities of the ISI- and the SPIKE-distance (Section 2.2), and contrast their local behavior to the global properties of the Victor-Purpura distance (Section 2.3). We evaluate their capability to distinguish different levels of spike train synchrony (Section 3.1) and compare their performance on two real datasets (Section 3.2). Finally, we describe the previously introduced measures against which we compare (Appendix A) and the data that we use (Appendix B). For completeness, in Appendix C we evaluate the performance of the new SPIKE-distance in the setups used in Kreuz et al. (2007, 2009).

2. Methods

2.1. The bivariate SPIKE-distance and its extensions

We denote with $\{t_i^{(n)}\} = t_1^{(n)}, ..., t_{M_n}^{(n)}$ the spike times and with M_n the number of spikes for neuron n with $n = 1, ..., N$.

2.1.1. Bivariate SPIKE-distance

For each neuron $n = 1, 2$ we assign to each time instant the time of the previous spike

$$t_{\mathrm{P}}^{(n)}(t) = \max(t_i^{(n)}|t_i^{(n)} \le t) \quad t_1^{(n)} \le t \le t_{M_n}^{(n)}, \quad (1)$$

and the time of the following spike

$$t_{\mathrm{F}}^{(n)}(t) = \min(t_i^{(n)}|t_i^{(n)} > t) \quad t_1^{(n)} \le t \le t_{M_n}^{(n)}, \quad (2)$$

as well as the interspike interval

$$x_{\mathrm{ISI}}^{(n)}(t) = t_{\mathrm{F}}^{(n)}(t) - t_{\mathrm{P}}^{(n)}(t). \quad (3)$$

We denote the instantaneous differences of previous and following spike times as

$$\Delta t_{\mathrm{P}}(t) = t_{\mathrm{P}}^{(1)}(t) - t_{\mathrm{P}}^{(2)}(t) \quad (4)$$

and

$$\Delta t_{\mathrm{F}}(t) = t_{\mathrm{F}}^{(1)}(t) - t_{\mathrm{F}}^{(2)}(t), \quad (5)$$

respectively, and the mean interspike interval (here $N = 2$) as
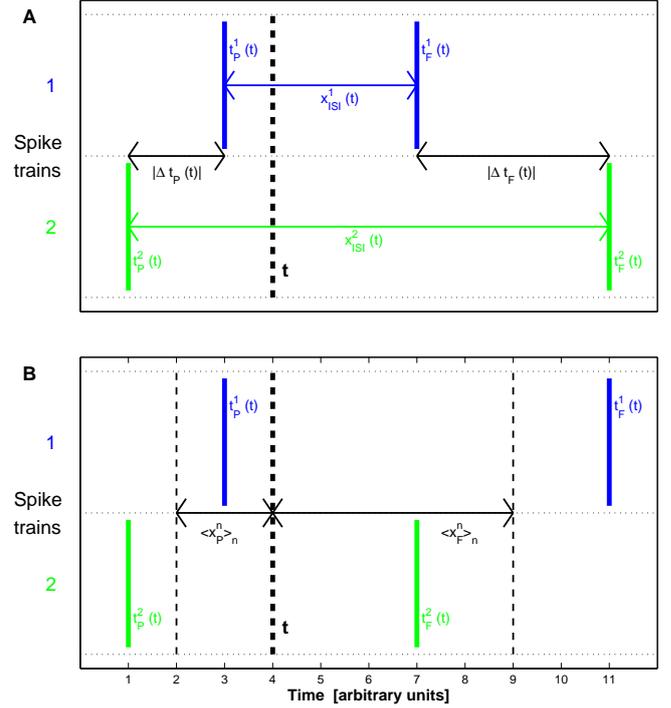

Fig. 1. (color online) Illustration of the bivariate SPIKE-distance. A. Time instant t and its relation to the previous spikes $t_P^{(n)}$ and the following spikes $t_F^{(n)}$ as well as their differences. In this example the interspike interval of the first spike train is included in the interspike interval of the second spike train. The spikes of the two spike trains as well as their ISIs are shown in blue and green, respectively. The time instant under consideration is marked by a vertical dashed line, whereas horizontal solid arrows indicate the absolute differences $|\Delta t_{\mathrm{P}}(t)|$ and $|\Delta t_{\mathrm{F}}(t)|$ between the previous and the next spikes, respectively. B. Illustration of the weighting of the two contributions by the distance to the previous and the following spikes. Here the second spike of the second spike train comes first. The average distances to the previous and to the following spikes are represented by horizontal black lines. Note that for both examples we get the same value $S(t) = 0.367$ (Eq. 11), since we just switched the following spikes which effected the individual intervals but not their sum.

$$\langle x_{\mathrm{ISI}}^{(n)}(t)\rangle_n = \frac{1}{N}\sum_{n=1}^{N} x_{\mathrm{ISI}}^{(n)}(t). \quad (6)$$

Note that by definition the intervals $\Delta t_{\mathrm{P}}(t)$ and $\Delta t_{\mathrm{F}}(t)$ do not cover the time instant t.

An instantaneous spike time based measure of spike train distance is given by the mean of the two absolute differences of previous and following spike times. In order to be time-scale independent (i.e., invariant to stretching and compressing the spike trains) we normalize this average difference by the mean interspike interval. This way we get the instantaneous spike difference (Fig. 1A)

$$S_2(t) = \frac{|\Delta t_{\mathrm{P}}(t)| + |\Delta t_{\mathrm{F}}(t)|}{x_{\mathrm{ISI}}^{(1)}(t) + x_{\mathrm{ISI}}^{(2)}(t)}. \quad (7)$$

The function $S_2(t)$ is piecewise constant taking just one value within each interval of the pooled spike train. In order to be more local in time, we weight the two terms $|\Delta t_{\mathrm{P}}(t)|$ and $|\Delta t_{\mathrm{F}}(t)|$ such that the difference of the spikes that are

closer dominate (Fig. 1B). To this aim we denote with

$$x_{\mathrm{P}}^{(n)}(t) = t - t_{\mathrm{P}}^{(n)}(t) \qquad (8)$$

and

$$x_{\mathrm{F}}^{(n)}(t) = t_{\mathrm{F}}^{(n)}(t) - t \qquad (9)$$

the distances to the previous and the following spikes for each neuron $n = 1, 2$ and with $\langle x_{\mathrm{P}}^{(n)}(t)\rangle_n$ and $\langle x_{\mathrm{F}}^{(n)}(t)\rangle_n$ the respective means over both neurons.

As can be seen in Fig. 1, the sum of these two values equals the mean interspike interval:

$$\langle x_{\mathrm{P}}^{(n)}(t)\rangle_n + \langle x_{\mathrm{F}}^{(n)}(t)\rangle_n = \langle x_{\mathrm{ISI}}^{(n)}(t)\rangle_n. \qquad (10)$$

From these quantities we obtain the instantaneous weighted spike difference as:

$$S(t) = \frac{|\Delta t_{\mathrm{P}}(t)|\langle x_{\mathrm{F}}^{(n)}(t)\rangle_n + |\Delta t_{\mathrm{F}}(t)|\langle x_{\mathrm{P}}^{(n)}(t)\rangle_n}{\langle x_{\mathrm{ISI}}^{(n)}(t)\rangle_n^2}. \qquad (11)$$

Finally, integrating over time yields the bivariate SPIKE-distance D_{S}:

$$D_{\mathrm{S}} = \frac{1}{T}\int_{t=0}^{T} S(t)dt. \qquad (12)$$

From Fig. 1 it is apparent that the sum of the two spike time differences cannot be larger than the sum of the two interspike intervals. Therefore, the bivariate SPIKE-distance is bounded in the interval $[0, 1]$. The value 0 is only obtained for perfectly identical spike trains.

2.1.2. Averaged bivariate SPIKE-distance

The averaged bivariate SPIKE-distance for a larger number of spike trains is the bivariate SPIKE-distance averaged over all pairs of neurons. The same kind of time-resolved visualization as in the bivariate case is possible, because the two averages over time and over pairs of neurons commute. We thus can first calculate the instantaneous average $S^{\mathrm{a}}(t)$ over all pairwise instantaneous weighted spike differences $S^{mn}(t)$ (Eq. 11)

$$S^{\mathrm{a}}(t) = \frac{1}{N(N-1)/2}\sum_{n=1}^{N}\sum_{m=n+1}^{N} S^{mn}(t) \qquad (13)$$

and then average over time

$$D_{\mathrm{S}}^{\mathrm{a}} = \frac{1}{T}\int_{t=0}^{T} S^{\mathrm{a}}(t)dt. \qquad (14)$$

Like the original SPIKE-distance, the averaged bivariate SPIKE-distance is restricted to the interval $[0, 1]$.

2.1.3. Multivariate SPIKE-distance

Calculating the average over pairs of spike trains can become very time-consuming as soon as the number of neurons N increases, since the computational cost scales with N^2. In such cases a multivariate approach which scales only with N is computationally preferable.

For each time instant we take the standard deviations over all previous and all following spike times and divide their mean by the mean instantaneous ISI:

$$S_2^{\mathrm{m}}(t) = \frac{(\sigma[t_{\mathrm{P}}^{(n)}(t)]_n + \sigma[t_{\mathrm{F}}^{(n)}(t)]_n)/2}{\langle x_{\mathrm{ISI}}^{(n)}(t)\rangle_n}. \qquad (15)$$

Similar to the bivariate case, in order to be more local in time we can weight the two terms such that the standard deviation of the spike times that are closer dominates. This way we obtain the instantaneous weighted spike standard deviation:

$$S^{\mathrm{m}}(t) = \frac{\sigma[t_{\mathrm{P}}^{(n)}(t)]_n\langle x_{\mathrm{F}}^{(n)}(t)\rangle_n + \sigma[t_{\mathrm{F}}^{(n)}(t)]_n\langle x_{\mathrm{P}}^{(n)}(t)\rangle_n}{\langle x_{\mathrm{ISI}}^{(n)}(t)\rangle_n^2}. \qquad (16)$$

Finally, the multivariate SPIKE-distance $D_{\mathrm{S}}^{\mathrm{m}}$ is obtained by integrating over time:

$$D_{\mathrm{S}}^{\mathrm{m}} = \frac{1}{T}\int_{t=0}^{T} S^{\mathrm{m}}(t)dt. \qquad (17)$$

The multivariate SPIKE-distance has 0 as a lower bound but does not have an upper bound and in particular can attain values larger than 1.

2.1.4. General remarks

Since $\langle x_{\mathrm{P}}^{(n)}(t)\rangle_n$ and $\langle x_{\mathrm{F}}^{(n)}(t)\rangle_n$ depend explicitly on the time instant t, all three types of instantaneous SPIKE-measures $S(t)$, $S^{\mathrm{a}}(t)$, and $S^{\mathrm{m}}(t)$ (Eqs. 11, 13, 16) are piecewise linear rather than piecewise constant. Thus a new value has to be calculated for each sampling point and not just once per each interval in the pooled spike train. However, this is only necessary when the localized visualization is desired. In case the distance value itself is sufficient, the short computation time can be even further decreased by representing each interval by the value of its center and weighting it by its length. This actually gives the correct result, the time-resolved calculation is a very good approximation for sufficiently small sampling intervals dt.

An alternative variant to the time-weighted average used in Eqs. 12, 14, and 17 is spike-weighted averaging where the SPIKE-distances are evaluated only after every new spike. This way each interval of the pooled spike trains contributes the same and not according to its length. For the sake of brevity in this study we restrict ourselves to presenting results of the time-weighted average only, although the spike-weighted variant occasionally (for example for the data analyzed in Section 3.2.2) exhibits slightly better results.

The Matlab source code for calculating and visualizing both the SPIKE- and the ISI-distances can be found under www.fi.isc.cnr.it/users/thomas.kreuz/sourcecode.html.

2.2. Motivation: Sensitivity to spike coincidences and the spike train of origin

The main difference between the SPIKE-based methods and the previously proposed ISI-based methods (cf.
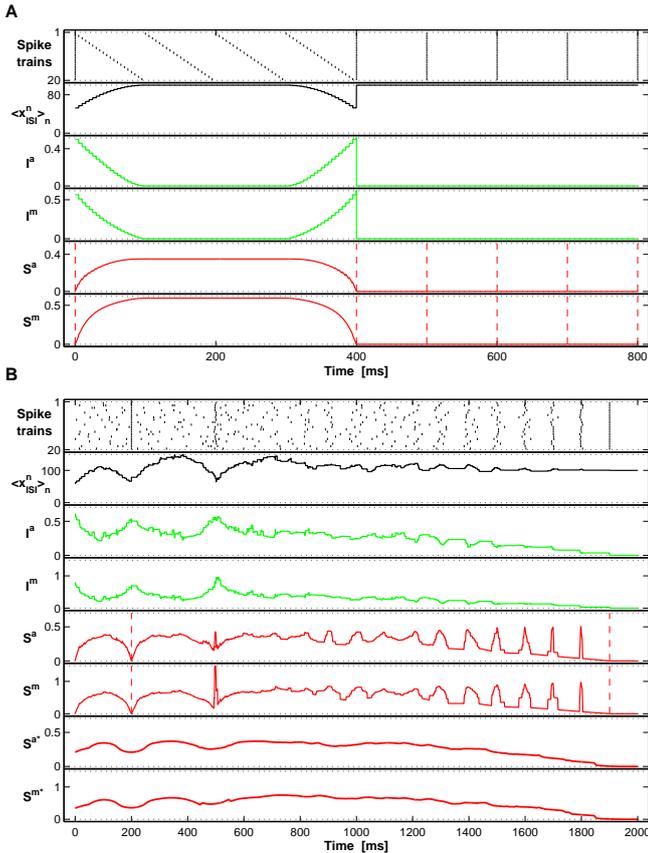
Fig. 2. (color online) Instantaneous ISI- and SPIKE-measures for constructed spike trains. On top we depict the spike trains and the mean instantaneous ISIs according to Eq. 3. Below that we show the four instantaneous measures (from top to bottom): the averaged bivariate ISI-ratio $I^{a}(t)$ (Eq. A.3), the multivariate coefficient of variation of the interspike intervals $I^{m}(t)$ (Eq. A.5), the weighted spike difference $S^{a}(t)$ (Eq. 11), and finally the weighted spike standard deviation $S^{m}(t)$ (Eq. 16). For the latter dashed vertical lines mark the occurrence of perfectly synchronous events. A. In the first interval all spike trains are regular, but with constant phase lags, then all spikes are regular with zero phase lag, i.e., identical. B. Spiking events with increasing jitter plus one noisy and one perfectly synchronous spiking event towards the end. For the instantaneous SPIKE-measures we also show the moving averages (of order 50 sampling intervals) at the bottom of this subplot.

Appendix A.1) is their different sensitivity to spike coincidences. The multiple spike trains shown in Fig. 2 were specifically constructed to illustrate this. In the first half ($< 400 \, \mathrm{ms}$) of Fig. 2a all 20 spike trains are regular but with constant phase lags, while in the second half ($400 - 800 \, \mathrm{ms}$) all spike trains are identical. Neither the averaged bivariate ISI-distance D^{a}_{I} nor the multivariate ISI-distance D^{m}_{I} distinguish between the intervals $100 - 300 \, \mathrm{ms}$ (the first interval without the transients) and $400 - 800 \, \mathrm{ms}$, since the instantaneous frequencies are the same thus yielding a value of zero in both cases. The SPIKE-distances D^{a}_{S} and D^{m}_{S} on the other hand do distinguish, and higher values are obtained for the first interval in which spikes are maximally dispersed, whereas the coincident spikes in the second interval yield zero values indicating perfect synchrony.

In the example of Fig. 2b we start with spike trains that are uncorrelated and basically random. At 200 ms and at

500 ms two events are inserted, the first one perfectly synchronous and the second one with a certain amount of jitter. Subsequently, the spike trains become more and more regular which is achieved by creating events every 100 ms with decreasing amounts of jitter and closing with a perfectly synchronous spiking event at 1900 ms.

The perfectly synchronous spiking event embedded within the noise (200 ms) is recognized only by the two instantaneous SPIKE-measures S^{a} and S^{m} which decrease to zero. On the other hand, the instantaneous ISI-measures even show peaks which are caused by the normalization. Similar peaks occur at the second unreliable event (500 ms). The SPIKE-measures on the other hand mark this event with a Mexican hat shaped event kernel [1]. The reason for the Mexican hat shape of these event kernels is intuitive: Right before the spiking event all differences between the following spike times are small as are all differences between the previous spikes right after the event. This affects respectively the first and the second half of the numerator entering the instantaneous dissimilarities (cf. Eq. 11). Accordingly, values are decreased with respect to the mean level. Furthermore, within the spiking event there is a small interval for which some of the spikes are still following spikes while others are already previous spikes. Thus for this small interval the respective differences between previous and following spike times are very large and so is the value of the instantaneous SPIKE-measures.

Subsequently, when the noise is gradually decreased, all measures, starting from a plateau with moderate fluctuations reflecting the initial inherent randomness, exhibit a consistent decrease. However, this drop occurs in a different manner for the instantaneous ISI- and SPIKE-measures. While the ISI-measures decrease rather gradually with only a few smaller elevations, the SPIKE-measures mark the events with a series of peaks. These peaks are no longer Mexican hat shaped because between the events there is no noisy background level to decline to. With the increasing reliability of the spike events the peaks are getting more and more prominent. Consequently, a perfectly synchronous event like the one at 1900 ms could be represented as a peak with infinitely small width and maximum amplitude. For such events the SPIKE-measures S^{a} and S^{m} yield the value zero (as expected for perfectly synchronous spike trains). The same value is also obtained for the intervals between two perfectly synchronous events. In order to distinguish these two cases we mark the occurrences of the perfect events by adding vertical dashed lines to the temporal profiles (see second half of Fig. 2A).

The instantaneous SPIKE-measures are sensitive to spike coincidences and assign specific signatures to their time of occurrence. However, in case the focus of attention lies on the long-term changes in spike train synchrony, an

---

[1] Here the expression "Mexican hat" is not meant to strictly describe the difference between two Gaussians, but is rather used in a general sense to describe the succession "plateau - small drop - high peak - small drop -plateau".
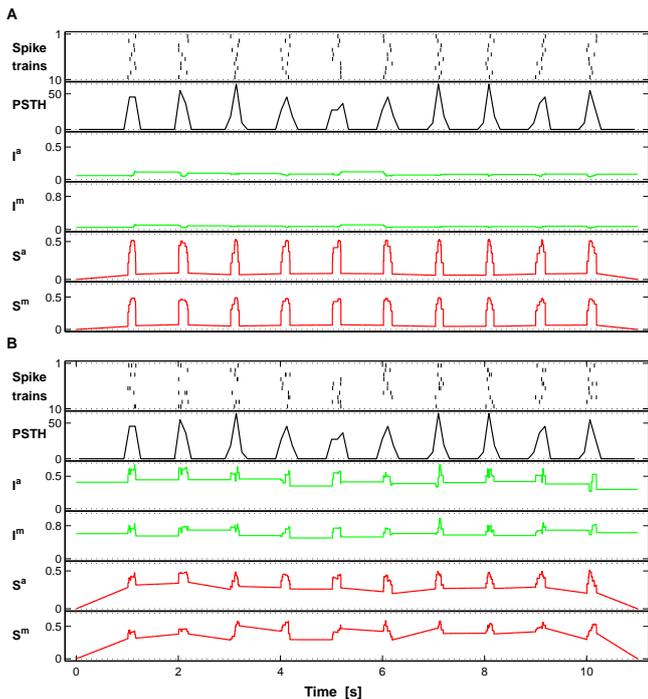
Fig. 3. Two sets of spike trains demonstrating the sensitivity of the instantaneous ISI- and SPIKE-measures to the spike train of origin. By construction the pooled spike train of the two sets is identical consisting of 10 regularly distributed bursts, only the distribution of the spikes among the individual spike trains differs. A. High reliability: Spikes from each burst are equally distributed among the spike trains. B. Irregular behaviour: All spikes are randomly assigned to the individual spike trains. Whereas the PSTH is by construction exactly identical in both cases, the ISI- and the SPIKE-distance can distinguish these cases resulting in low distances in the first case and in higher distances in the second case.

appropriate moving average eliminates these short time-scale signatures and a gradual decrease similar to the one of the ISI-measures is obtained (cf. the two lowest subplots of Fig. 2B).

The SPIKE-distances are not only sensitive to the timing of the individual spikes, but also to their spike train of origin (Fig. 3). To show this, we start with one spike train consisting of 10 equally distributed bursts of 10 spikes each. From this spike train we construct two sets of $N = 10$ spike trains with $M_n = 10$ spikes each. This is achieved by assigning the individual spikes to their spike train of origin which is the inverse operation to pooling spikes from several spike trains. In the first set the spikes are distributed such that we have 10 unreliable events with one spike in each spike train (Fig. 3A), while in the second set the spikes are assigned to random spike trains keeping only the number of $M_n = 10$ spikes per spike train constant (Fig. 3B). As can be seen in the four lower traces, both the ISI- and the SPIKE-distances can clearly distinguish these qualitatively different behaviors. This is in contrast to the Peri-Stimulus Time Histogram (PSTH) which, like all other measures of spike train synchrony based on the PSTH or on the pooled spike train in general, is invariant to shuffling spikes among the spike trains.
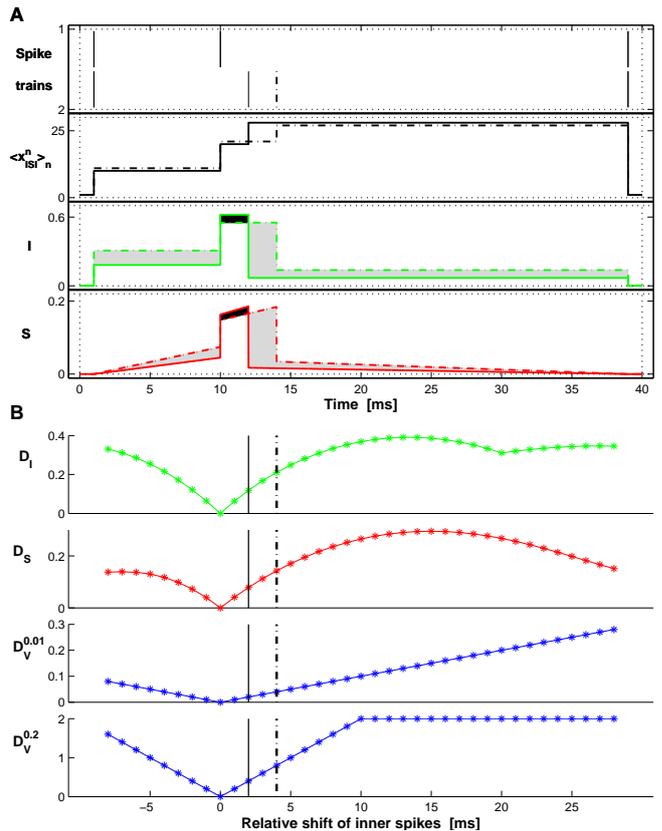

Fig. 4. (color online) Local behaviour of SPIKE-distances. A. All spikes are set to fixed positions except for the inner spike of the second spike train which is shifted relative to the inner spike of the first spike train. In this example this spike is shifted from 12 ms (solid lines) to 14 ms (dashed lines). Following the spike trains and the mean instantaneous ISI-values we depict the bivariate ISI-ratio $I(t)$ and the mean spike difference $S(t)$. For these two profiles the positive and negative instantaneous changes are marked by bright and dark shaded areas, respectively. In this example these two opposing contributions sum up to an increase of the distances. B. Dependence of the ISI distance D_I, the SPIKE-distance D_S and the Victor-Purpura distance D_V (for cost parameters c_V equal to 0.01 and 0.2) on the relative shift of the two inner spikes. The relative positions of the spikes in A are marked by vertical lines.

2.3. Properties: Local behavior

In order to illustrate the local behavior of the time-resolved ISI- and SPIKE-distances and compare it with the global behavior of the Victor-Purpura distance (cf. Appendix A.2), we start with a simple example (Fig. 4) composed of two identical spike trains with just three spikes each. Then, while all other spikes are kept fixed, the inner spike of the second spike train is shifted in time.

Exemplary spike trains and the results for the time-resolved bivariate measures $I(t)$ and $S(t)$ are shown in Fig. 4A. Both measures show local signatures that are somehow counter-intuitive: They assign larger positive deviations for more closer spikes. The reason is as follows: As the difference between the two inner spikes increases, the value of the instantaneous dissimilarities in the interval between these spikes (the peak height of the event kernel) decreases, however, at the same time the support interval of the peak

value is getting longer as are the dissimilarity values in the remaining intervals (the drop height of the event kernel) although their support is getting smaller. Initially the sum effect is positive (compare the dark and the bright areas), however, as the difference between the two spikes is getting even larger, the relative importance of these two opposing effects changes. Accordingly, the corresponding distances D_{I} and D_{S} shown in Fig. 4B exhibit an initial increase which then leads to a maximum value for an intermediate shift followed again by a decrease. As the different slopes of the initial increase in distance for positive and negative shifts prove, the relative importance of the two opposing effects does not only depend on the shift between the two intermediate spikes, but is also influenced by the relative lengths of the outer intervals.

One peculiarity can be observed for the ISI-distance D_{I}, a local minimum for a shift of 20 ms. This is the point for which the two spike trains are symmetric under time reversal. Accordingly, in the central interval between the two inner spikes the instantaneous measure $I(t)$ equals zero and this leads to the low value of D_{I}.

In Fig. 4B we also show results of the Victor-Purpura distance D_{V} for two cost values $c_{\mathrm{V}} = 0.01$ and $c_{\mathrm{V}} = 0.2$. A linear increase can be observed with the slope of the increase given by the cost parameter. Note that no distance values higher than 2 can be obtained, since for high costs and large differences of the two inner spikes shifting gets too expensive and it becomes more affordable to delete and to insert the spike for a cost of 2.

The difference between the instantaneous measures and the Victor-Purpura distance stems from the fact that the first are local and the latter is global. For the SPIKE-distance the inner spike of the second spike train is approaching the third spike of the first spike train which leads to the effect that the two spike trains are getting more similar again. The Victor-Purpura distance on the other hand matches the two third spikes and thus considers only the difference between the two inner spikes although they are further apart than the later spikes.

3. Results

3.1. Simulation: Capability to distinguish different levels of spike train synchrony

As a first quantitative test for the different measures we evaluated whether they are able to track continuous changes in synchrony when the transition to synchrony is based on coincidences of spike times. Measures comprise the bivariate and multivariate ISI- and SPIKE-distances $D_{\mathrm{I}}^{\mathrm{a}}$, $D_{\mathrm{I}}^{\mathrm{m}}$, $D_{\mathrm{S}}^{\mathrm{a}}$, and $D_{\mathrm{S}}^{\mathrm{m}}$ as well as the Victor-Purpura distance D_{V}. The latter measure is here represented by just one cost value $c_{\mathrm{V}} = 0.2$, other values yielded equivalent results. As a measure frequently used in real data applications we also included the correlation coefficient C (cf. Appendix A.3) whose performance was optimized over different values of

the bin size.

We generated 25 spike trains with 100 spikes each. The spikes were randomly distributed within the interval $[0, 1]$ using a sampling interval of 0.0001. In order to create spike trains with increasing levels of correlations we followed a correlation scheme introduced in Kreuz et al. (2006) and defined a matching parameter m that governed the fraction of shared spikes for each pair of neurons: for matching $m = 0$ all spikes are randomly distributed, whereas for matching $m = 1$ all spike trains are identical.

Average values and standard deviations over 100 realizations are shown in Fig. 5A. All distances equal 0 for a perfect matching ($m = 1$). For decreasing matchings all average values increase monotonically, however, the shape of the increase differs. The multivariate methods first show a very steep and then a rather moderate increase. The averaged bivariate methods exhibit a more gradual increase except for the averaged bivariate ISI-distance whose increase is rather slow for low matchings. Furthermore, as indicated by the standard deviations of the distributions, the averaged bivariate methods are characterized by considerably narrower distributions with the only exception being the Victor-Purpura distance which exhibits the broadest distributions of all measures. The average bivariate SPIKE-distance $D_{\mathrm{S}}^{\mathrm{a}}$ and the optimized correlation coefficient are the only measures to combine a rather constant increase with a low variability.

Similar to the analysis of Kreuz et al. (2009) (see also Appendix C.2) we quantified the capability of the measures to distinguish distributions with neighboring matchings using Kolmogorov-Smirnov statistics (Fig. 5B). For the averaged bivariate SPIKE-distance as well as for the optimized correlation coefficient the maximum value of 1 is obtained indicating pairs of non-overlapping neighboring distributions. For the other measures deviations from 1 indicate overlapping distributions. This is quantified by the average of the Kolmogorov-Smirnov statistics over all matching transitions (Fig. 5C). Perfect scores are obtained for the averaged bivariate SPIKE-distance and the optimized correlation coefficient followed by the averaged bivariate ISI-distance. In general the multivariate measures yield lower averages with the ISI-distance again lagging behind the SPIKE-distance. The only exception is the Victor-Purpura distance which exhibits the lowest capability to distinguish different levels of spike train synchrony.

3.2. Application to real data

In Section 3.2.1 we investigate the spike train similarity within a complete population of retinal ganglion cells, while in Section 3.2.2 we evaluate how well the various measures can discriminate single-unit responses to different taste stimuli. Since in both applications we use setups which involve only similarities between pairs of spike trains, we only compare the basic bivariate measures and not the averaged bivariate or multivariate extensions. Thus

Fig. 6. A. Receptive fields of an almost complete population of $N = 105$ ON-Parasol retinal ganglion cells. B. Spike trains from these 105 cells during the first two seconds of one realization of white noise stimulation.
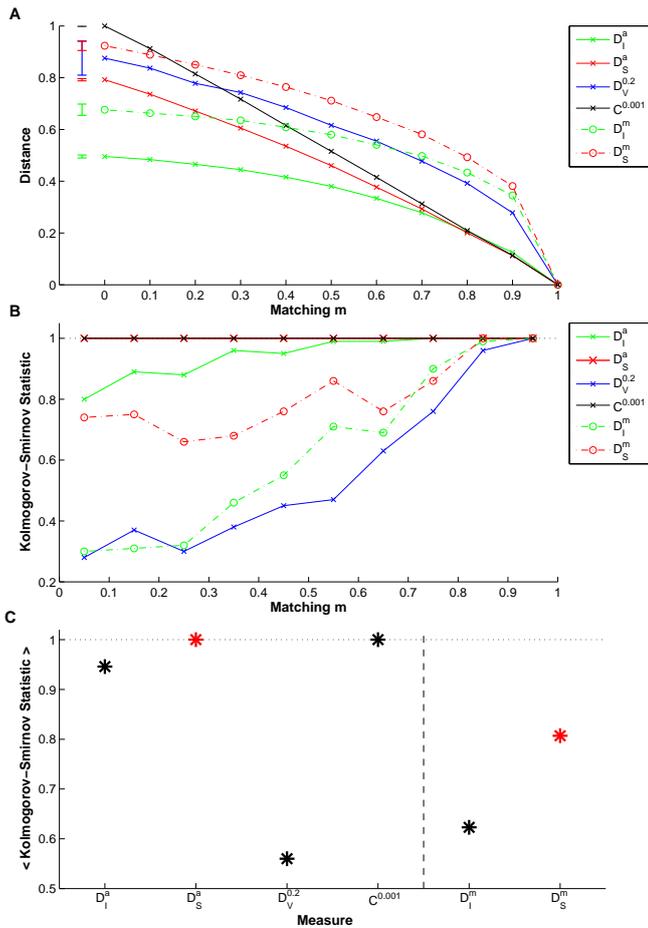
Fig. 5. (color online) Capability to distinguish different levels of spike train synchrony. A. ISI- and SPIKE-distances as well as Victor-Purpura distance and correlation coefficient versus the matching parameter. Values shown are averages and standard deviations of distributions from 100 realizations with $N = 25$ spike trains and $M = 100$ spikes each. For clarity we only show the standard deviations for matching $m = 0$, the other standard deviations decrease monotonously with the matching. B. Kolmogorov-Smirnov statistics showing the distinguishability of distributions with neighboring matchings. Values for the different measures are plotted against the mean matching of the respective two distributions. C. Comparison of measures: Kolmogorov-Smirnov statistics averaged over all neighboring matchings. The vertical line seperates the averaged bivariate and the multivariate measures.

the measures are narrowed down to the ISI-distance D_{I}, the SPIKE-distance D_{S}, the Victor-Purpura distance D_{V} [2], and the correlation coefficient C. In both applications for D_{V} and C we sampled the relevant range of the respective time-scale parameter equidistantly on a logarithmic scale.

3.2.1. *Spike train similarity among retinal ganglion cells*

We first applied the bivariate spike train distances to responses from an almost complete population ($N = 105$ neurons) of ON parasol retinal ganglion cells (Shlens et al., 2006, 2009; for more details on the data confer Appendix

---

[2] Note that among the time-scale dependent spike distances we restrict ourselves to the Victor-Purpura distance, since this was the measure that proved to be the best performer in previous measure comparisons (Kreuz et al. (2007, 2009), see also Appendix C).
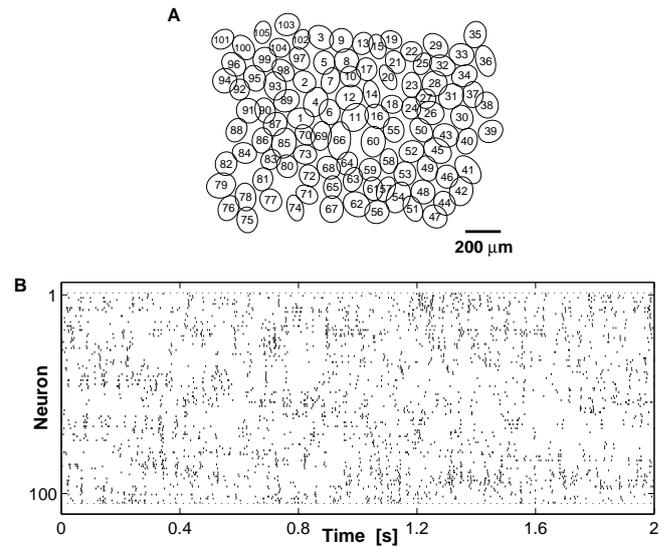
B.1). These recordings were performed using both white noise stimulation and constant, spatially uniform illumination. As can be seen in Fig. 6A, the receptive fields of the complete population form an orderly mosaic that tiles visual space with minimal overlap. Exemplary snapshots of the spiking activity of the population responding to a white noise stimulation are shown in Figs. 6B. This white noise stimulation was also used to identify the receptive field of the retinal ganglion cells by means of reverse correlation Chichilnisky (2001).

From this mosaic we extract the pairwise distances between the centers of the respective fields. It is well known that correlations systematically decrease with the distance between the two neurons' receptive fields (Mastronarde, 1983; Meister et al., 1995; De Vries, 1999; Shlens et al., 2006). Here we can use this behavior as benchmark and evaluate whether the spike train distances yield higher values for pairs of neurons with larger distances between their receptive fields (and vice versa for the correlation coefficient C).

For each of these measures and for both kinds of stimulations we first calculated all pairwise spike train distances for the complete population. Exemplary scatter plots of the measures versus the distance between the receptive fields are shown for one realization of the white noise stimulation in Fig. 7. All measures exhibit a very clear initial dependency but show a pronounced saturation for higher distances between RFs. What differs between the measures is the distance between RFs at which the transition between these two qualitatively behaviors takes place. While it is rather low for the Victor-Purpura distance and the ISI-distance, it is much larger for the SPIKE-distance and the correlation coefficient.

For all measures we quantified the relation between the spike train distances and the distances between the receptive fields using the absolute Spearman's rank correlation
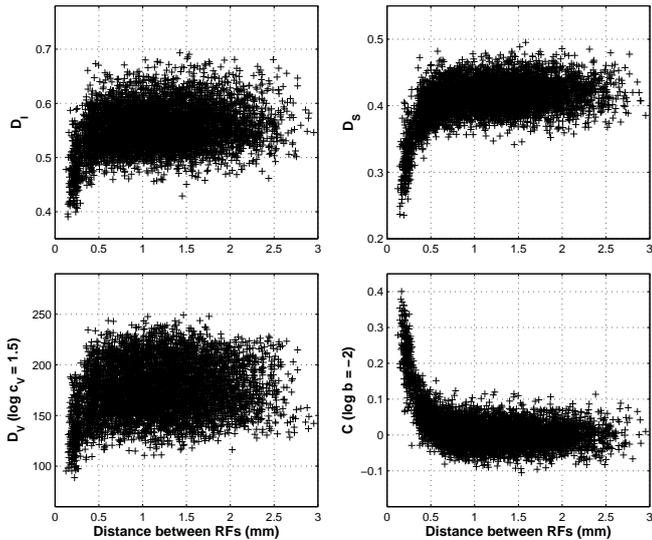
Fig. 7. Scatter plots of the ISI-distance D_I, the SPIKE-distance D_S, the Victor-Purpura distance D_V (for $\log c_V = 1.5$), and the correlation coefficient C (for $\log b = -2$) versus the distance between the centers of the receptive fields (RFs). Note that C is a measure of similarity and thus exhibits a decrease with the distance between the RFs. For both D_V and C we show the plots for the parameter value that yielded the highest absolute Spearman's rank correlation coefficient R (cf. Fig. 8). The values of R for these example were 0.23 (D_I), 0.36 (D_S), 0.17 (D_V), and 0.39 (C), respectively.

coefficient R (Fig. 8). For both the white noise stimulation and the constant, spatially uniform illumination the highest mean correlations are obtained for the optimized correlation coefficient C. This is closely followed by the SPIKE-distance D_S which in turn yields a considerable improvement over the ISI-distance D_I. For the Victor-Purpura distances D_V despite the optimization the highest coefficient is considerably lower than the values obtained for the other methods. Also results are not very robust since a more detailed investigation revealed that for different realizations the actual maximum R-value was attained for cost values covering two entire logarithmic decades.

3.2.2. *Taste stimuli discrimination from single-unit recordings*

As a second application to real data we analyze one complete dataset from "neurodatabase.org" (Gardner, 2004). It consists of single-unit responses of three neurons (#4, #9, and #11) in the nucleus of the solitary tract (NTS) of rats to four different taste stimuli (Di Lorenzo and Victor, 2003). For the three different neurons we have $N_R = 19$, 23, and 16 repetitions, respectively, for each stimulus. For more details on the data confer Appendix B.2.

For all measures and for each neuron separately we calculate the pairwise distance matrix for all $4 \cdot N_R$ realizations. Assuming stimulus-driven synchronization, a good discrimination should yield low distance values for responses to the same stimuli and high distance values to responses for different stimuli (and vice versa for the correlation coefficient).
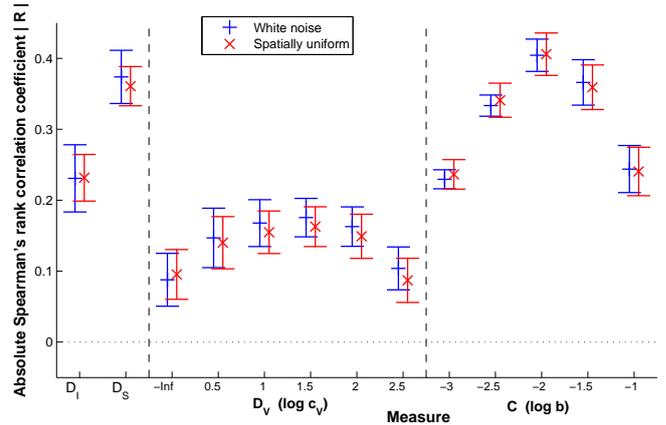

Fig. 8. Comparison of the absolute Spearman's rank correlation coefficients (average and standard deviation) over 18 presentations (10 s each) for both white noise stimulation and constant, spatially uniform illumination. Measures comprise the ISI- and the SPIKE-distance, the Victor-Purpura distance, and the correlation coefficient. The parameters of the latter two measures are varied on a logarithmic scale.

In order to evaluate the separation of the spike trains into 4 different clusters, we follow Victor and Purpura and define the distance between the spike train S_i and the cluster C_α as $\langle d(S_i, S_j)\rangle_\alpha$, where $\langle \cdot \rangle_\alpha$ denotes the average over all spike trains in the cluster C_α. From these distances we compute the normalized confusion matrix $p_{\alpha\beta}$ (Abramson, 1963; Victor and Purpura, 1996) whose entry $p_{\alpha\beta}$ is defined as the probability that C_β is the closest cluster to a spike train belonging to C_α. For a perfect clustering the confusion matrix is diagonal, whereas each misclassification increments a non-diagonal element. The performance of the measures in discriminating the different stimuli is finally quantified by the normalized mutual information

$$I_C = \left(\sum_{\alpha,\beta} p_{\alpha\beta} \log \frac{p_{\alpha\beta}}{P_\alpha P_\beta} \right) / I_{max} \qquad (18)$$

where $P_\alpha = \sum_b p_{\alpha b}$, and $P_\beta = \sum_b p_{b\beta}$ and I_{max} denotes the maximum mutual information obtained for a correct classification.

Results for the three neurons recorded during the taste stimuli discrimination task (Di Lorenzo and Victor, 2003) are shown in Fig. 9. For all three neurons the highest discrimination is obtained for the Victor-Purpura distance, however, as already reported in Di Lorenzo and Victor (2003) for different neurons the best discrimination is obtained for different coding schemes. The neurons #4 and #11 exhibit their maximum for positive values of the cost parameter indicating that a temporal coding scheme allow for greater discrimination of the four stimuli. Only for neuron #9 the curve does not increase considerably for positive cost parameters. In this case the spike timing is less relevant and a rate coding scheme is sufficient for a proper discrimination of the tastants. Slightly below the maximum I_C-values obtained for the Victor-Purpura distance follow the time-scale adaptive ISI-distance and SPIKE-distance. In this task there seems to be no clear distinction between
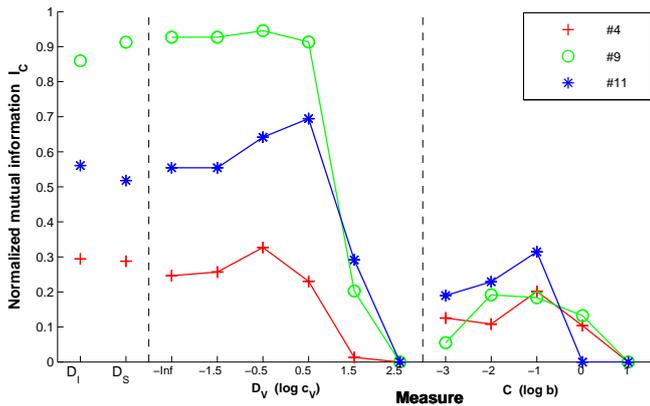
Fig. 9. Normalized confusion mutual information for three neurons responding to different taste stimuli. The same measures as in Fig. 8 were evaluated, only the range of the time-scale parameters was adapted in order to cover the maxima of discrimination for this task.

their discrimination values regardless of the neuron's coding scheme. Finally, for all three neurons the lowest discrimination capabilities are obtained by the correlation coefficient.

4. Discussion

Motivated by the prevalence of coincident spiking in many different areas of the brain, we propose a SPIKE-distance which, together with its multi-neuron extensions, can be applied to quantify the (dis)similarity of two or more spike trains. These measures are sensitive to the timing of spikes and are thus complementary to the ISI-distance (Kreuz et al., 2007) and its extensions (Kreuz et al., 2009) which are instead sensitive to the relative lengths of simultaneous interspike intervals.

At the same time the SPIKE-distance and its extensions share many distinct properties with the ISI-distance, in particular, they are parameter free and time-scale adaptive. The latter property can be preferable in applications to real data for which there is no validated knowledge about the relevant time scales. While time-scale dependent measures yield a functional characterization of the spike trains, a single valued method gives a more objective and comparable estimate of neuronal variability. Other drawbacks of time-scale dependent measures are the computational cost and the time and effort that is needed to find the right parameter. Moreover, it is not at all guaranteed that there exists a right parameter. For example, spike trains that include different time-scales such as regular spiking and bursting might result in misleading conclusions, since any fixed parameter will misrepresent either one of those dynamics.

One of the main arguments for the use of a time-scale dependent measures is their potential insight into the precision of the neuronal code (Victor and Purpura, 1996). A very common setup in experimental neuroscience is the recording of single- or multi-unit spike train responses for the repeated presentation of different classes of stimuli (for an overview see Victor and Purpura, 2005). The pairwise distance matrices over all realizations are calculated and used as input for a cluster analysis of the type used in Section 3.2.2. The time-scale for which the responses to different stimuli are best discriminated is then assumed to be the precision of the neural code. However, a recent investigation of this kind of precision analysis (Chicharro et al., 2011) has shown that the optimal time-scale obtained from the cluster analysis is far from being conclusive, but rather results in a non-trivial way from the interplay of different factors. These factors include the distribution of the information contained in different parts of the response and the degree of redundancy between them. For dynamic stimuli the optimal time scale also depends on the stimuli statistics, in particular, the temporal distribution of the stimulus features to which the neurons respond.

Despite the problems in the interpretation of the optimal time-scale, the Victor-Purpura distance is designed to test for specific codes ranging from a rate code to a coincidence detector (Victor and Purpura, 1997). The correlation coefficient focusses purely on the coincidences and thus reflects the most specific coding assumption. On the other extreme, the most general approach is taken by the ISI-distance and the SPIKE-distance which, in contrast to the Victor-Purpura distance, are time-scale adaptive and parameter-free. Thus the different measures can be ordered from measures tied to a specific hypothesis about the code (correlation coefficient) via intermediate measures (Victor-Purpura distance) to measures that are very general (ISI- and SPIKE distance). Measures on different ends of this scale are complementary in nature. The ones capable of quantifying the degree of dissimilarity of the spike trains without relying on specific coding hypotheses are very well suited for an exploratory analysis. Oppositely, once a particular coding scheme is hypothesized more specific measures are needed for a confirmatory analysis.

In the application to the retina data presented in Section 3.2.1 the correlation coefficient, which is focussed on spike coincidences, yields the best results. On the other hand, in Section 3.2.2 the same measure fails to discriminate the different taste stimuli. The former result is consistent with the prevalence of synchronized firing in the retina (Shlens et al., 2008), while in the latter taste discrimination task the distinction seems to rely on coding schemes other than coincidences (Di Lorenzo and Victor, 2003). The more general ISI- and SPIKE-distances show a very adaptive behavior and yield a good performance in both applications. It should be noted that while both measures discriminate the taste stimuli about equally well, the SPIKE-distance outperforms the ISI-distance on the retina data. This is consistent with the previous observation: When synchronized firing is prevalent, the sensitivity to spike coincidences exhibited by the SPIKE-distance becomes relevant and leads to a considerable improvement with respect to the ISI-distance.

Both ISI- and SPIKE-distance are conceptually simple, computationally efficient and easy to visualize in a time-resolved manner. This kind of visualization can be achieved because the distances are defined as temporal averages over

time profiles, i.e., they are based on instantaneous values which are calculated from the sequences of spike times. However, it should be noted that each instantaneous value cannot be interpreted without looking at its local context. The SPIKE-distances are time-resolved only in the sense that they assign to each spiking event an event kernel. In case the focus of attention is on the long-term behavior, these local event kernels can easily be eliminated by appropriate moving averaging (as shown in Fig. 2b). Another caveat regarding all measures of spike train synchrony is that they generally assume a zero time delay between spike trains. Accordingly, in case of a non-zero time delay, e.g., caused by finite signal transmission times between different brain regions, it should be detected and eliminated beforehand (Waddell et al., 2007; Nawrot, 2003).

The measures used in this study quantify the level of synchrony within one set of two or more spike trains. For the Victor-Purpura and the van Rossum distances (van Rossum, 2001, cf. Appendix C) there also exist extensions that estimate the synchrony between two populations of neurons (Aronov, 2003 and Houghton and Sen, 2008, respectively). Corresponding extensions for both the ISI- and the SPIKE-distance will be presented in a forthcoming study (Kreuz et al., 2011).

We close by pointing out once more that the Matlab source code for calculating and visualizing both the ISI- and the SPIKE-distances can be downloaded at www.fi.isc.cnr.it/users/thomas.kreuz/sourcecode.html.

Appendix A. Previously published measures of spike train distance

Here we restrict ourselves to descriptions of the ISI-distance together with its extensions, the Victor-Purpura distance, and the correlation coefficient since these are the measures that we deal with in more detail. For the other measures that we compare against in Appendix C please refer to the Appendix of Kreuz et al. (2009).

A.1. *The bivariate ISI-distance and its extensions*

The ISI-distance (Kreuz et al., 2007) and its extensions (Kreuz et al., 2009) are based on the instantaneous interspike intervals.

A.1.1. *Bivariate ISI-distance*

To define a time-resolved, symmetric, and time-scale adaptive measure of the relative firing rate pattern (Kreuz et al., 2007) we take the instantaneous ratio between $x_{\text{ISI}}^{(1)}$ and $x_{\text{ISI}}^{(2)}$ (Eq. 3), and combine according to:

$$I_{12}(t) = \begin{cases} x_{\text{ISI}}^{(1)}(t)/x_{\text{ISI}}^{(2)}(t) - 1 & \text{if } x_{\text{ISI}}^{(1)}(t) \le x_{\text{ISI}}^{(2)}(t) \\ -(x_{\text{ISI}}^{(2)}(t)/x_{\text{ISI}}^{(1)}(t) - 1) & \text{otherwise.} \end{cases}$$

$$(A.1)$$

This quantity becomes 0 for identical ISI in the two spike trains, and approaches -1 and 1, respectively, if the first or the second spike train is much faster than the other.

The bivariate ISI-distance is obtained by averaging the absolute ISI-ratio over time:

$$D_{\text{I}} = \frac{1}{T} \int_{t=0}^{T} dt |I_{12}(t)|. \qquad (A.2)$$

The bivariate ISI-distance is bounded in the interval $[0, 1]$.

A.1.2. *Averaged bivariate ISI-distance*

As in the case of the averaged bivariate SPIKE-distance (Section 2.1.2) the averages over pairwise distances and over time commute and we can visualize the instantaneous average in a time-resolved way. First we calculate the instantaneous average $A(t)$ over all pairwise absolute ISI-ratios $|I_{mn}(t)|$ (cf. Eq. A.1)

$$I^{\text{a}}(t) = \frac{1}{N(N-1)/2} \sum_{m=1}^{N} \sum_{n=m+1}^{N} |I_{mn}(t)| \qquad (A.3)$$

before we average over time:

$$D_{\text{I}}^{\text{a}} = \frac{1}{T} \int_{t=0}^{T} dt I^{\text{a}}(t). \qquad (A.4)$$

As the original measure, the averaged bivariate ISI-distance is restricted to the interval $[0, 1]$.

A.1.3. *Multivariate ISI-distance*

We derive a multivariate measure by calculating the instantaneous coefficient of variation taken across all neurons at any given instant in time

$$I^{\text{m}}(t) = \frac{\sigma[x_{\text{ISI}}^{(n)}(t)]_n}{\langle x_{\text{ISI}}^{(n)}(t)\rangle_n} \qquad (A.5)$$

and averaging over time:

$$D_{\text{I}}^{\text{m}} = \frac{1}{T} \int_{t=0}^{T} dt I^{\text{m}}(t). \qquad (A.6)$$

For identical spike trains D_{I}^{m} obtains the same lower bound of zero as D_{I} and D_{I}^{a}, but unlike them it lacks an upper bound.

A.2. *Victor-Purpura distance*

The spike train distance D_{V} introduced in Victor and Purpura (1996) defines the distance between two spike trains in terms of the minimum cost of transforming one spike train into the other by using just three basic operations: spike insertion, spike deletion and spike shift. While the cost of insertion or deletion of a spike is set to one, the cost c_{V} of moving a spike by some interval is the only parameter of the method, and sets the time-scale of the analysis. For zero cost, the distance is equal to the difference in spike counts, for high costs, the distance approaches the number of non-coincident spikes, as it becomes more favorable to delete all non-coincident spikes than to shift them.

Thus, by increasing the cost, the distance is transformed from a rate distance to a timing distance. For multi-neuron data, synchrony is defined as the average over all pairs of spike trains:

$$D_{\mathrm{V}}^{\mathrm{a}} = \frac{1}{N(N-1)/2} \sum_{m=1}^{N} \sum_{n=m+1}^{N} D_{\mathrm{V}}^{mn}. \qquad (A.7)$$

A.3. *Correlation coefficient*

In contrast to all the other measures used in this paper the bivariate correlation coefficient relies on binning with the bin size b as a free parameter. If there is no spike within the bin, a zero is assigned, otherwise this bins' value is set to one [3]. The two resulting vectors $\overrightarrow{b}_x$ and $\overrightarrow{b}_y$ are used as input for the correlation coefficient C which equals the normalized covariance function c according to

$$C = c(\overrightarrow{b}_x, \overrightarrow{b}_y)/\sqrt{c(\overrightarrow{b}_x, \overrightarrow{b}_x) \cdot c(\overrightarrow{b}_y, \overrightarrow{b}_y)}. \qquad (A.8)$$

Also the multi-neuron correlation coefficient is calculated by averaging over all pairs of spike trains.

Appendix B. Data

B.1. *Multi-neuron recordings from retinal ganglion cells*

In Section 3.2.1 the recorded activity of a nearly complete population of ON parasol retinal ganglion cells (RGCs) is used to compare the performance of the new SPIKE-distances with previously published measures such as the Victor-Purpura distance and the ISI-distances. The amount of synchronized firing between pairs of RGCs of the same type declines systematically with distance between the two cells (Mastronarde, 1983; Meister et al., 1995; De Vries, 1999; Shlens et al., 2006). This well described behavior was used as a benchmark against which the capability of the various measures was tested to assign higher distances to more distant cell pairs.

Retinas were obtained and recorded as described previously (Litke et al., 2004; Field et al., 2007). Briefly, eyes were enucleated from terminally anesthetized macaque monkeys (Macaca mulatta) used in the course of other experiments, in accordance with Salk Institute IACUC guidelines for the care and use of animals. Immediately after enucleation, the anterior portion of the eye and vitreous were removed in room light. Following a dark-adaptation period, segments of peripheral retina were isolated and placed flat, RGC layer down, on a planar array of 512 extracellular microelectrodes, covering an area of 1800×900 μm. During recording, the retina was perfused with Ames'

solution ($32 - 34\,^{\circ}C$) bubbled with 95 % O2 and 5 % CO2, pH 7.4.

Recordings were analyzed offline to isolate the spikes of different cells, as described previously (Field et al., 2007). Briefly, candidate spikes were detected using a threshold on each electrode, and the voltage waveforms on the electrode and nearby electrodes around the time of the spike were extracted. Clusters of similar spike waveforms were identified as neurons if they exhibited a refractory period.

Visual stimulation techniques were described previously (Field et al., 2007). Briefly, the optically reduced image of a linearized cathode ray tube computer display (Sony Multiscan E100) refreshing at 120 Hz was focused on the photoreceptor outer segments. Recordings were performed at a low photopic light level (1140, 1150, 620 P* per L, M, S cone per sec). The photopic photon absorption rates were computed assuming a $0.37 \mu m^2$ collecting area for primate cones (Schnapf et al., 1990).

Spatiotemporal receptive fields were measured using reverse correlation with a white noise stimulus, composed of a lattice of square pixels updating randomly and independently over time (Chichilnisky, 2001). The intensity of each display primary at each pixel location was chosen independently from a binary distribution at each refresh. The time-averaged contrast of each primary (difference between the maximum and minimum intensities divided by the sum of intensities) was 96%. A stimulus pixel size of 60 μm on a side was used. Measurements of synchronized firing were obtained in the presence of a spatially uniform, full-field display with intensity equal to the mean intensity of the white noise stimulus used for receptive field characterization.

ON parasol cells were identified by their size, their response kinetics, and their receptive field characteristics (Chichilnisky, 2002). The spatial receptive field was summarized by an elliptical two-dimensional Gaussian function. The outlines in Fig. 6A represent the 1 SD boundary of the Gaussian fits. The receptive fields of all ON parasol cells form an orderly mosaic that tiles visual space with minimal overlap. This completeness of the mosaics indicates that the recordings sampled most of the parasol cells over the electrode array. The distance between cells was normalized by the mean SD of their Gaussian fits measured along the line connecting the centers of the fits.

Responses to two kinds of stimulations were analyzed. For both white noise stimulation and constant, spatially uniform illumination we analyzed 18 segments of 10 s each which were distributed regularly over a time scan of 30 minutes.

B.2. *Taste response and temporal coding in the nucleus of the solitary tract of the rat*

In Section 3.2.2 we compare the performance of the spike train distances in discriminating four different taste stimuli. In Di Lorenzo and Victor (2003) the authors exam-

---

[3] Note that this binary setup of the correlation coefficient disregards all differences within the bin size as well as all differences larger than the bin size (similar to a rectangular kernel), whereas both the Victor-Purpura and the SPIKE-distance weight all spike time differences linearly (similar to a triangular kernel).

ined the reliability of response rate across stimulus repetitions and the potential contribution of temporal coding to the discrimination of four taste stimuli (NaCl, sucrose, quinine HCl, and HCl) in the nucleus of the solitary tract (NTS) of rats. A selected dataset consisting of responses recorded from three different neurons is available online (http://neurodatabase.org/, Gardner, 2004) as experiment "dilorenzo-ndb-1181". For each of the four stimuli recordings of these cells, labeled #4, #9, and #11, include 19, 23, and 16 repetitions, respectively.

B.3. *Hindemarsh-Rose simulations*

The spike trains of the controlled configuration used in Appendix C were generated using time series extracted from a network of Hindemarsh-Rose neurons (Hindmarsh and Rose, 1984). This network was originally designed to analyze semantic memory representations using feature-based models. Details of the network architecture and the implementation of the feature coding can be found in Morelli et al. (2005). The clustering properties of these data were detailed in Kreuz et al. (2007), their set separation was investigated in Kreuz et al. (2009), and we here follow the description of these data given in Kreuz et al. (2009).

In short, the state of the neuron n was determined by three dimensionless first-order differential equations describing the evolution of the membrane potential X_n, the recovery variable Y_n, and a slow adaptation current Z_n,

$$\dot{X}_n = Y_n - X_n^3 + 3X_n^2 - Z_n + I_n + \alpha_n - \beta_n \tag{B.1}$$

$$\dot{Y}_n = 1 - 5X_n^2 - Y_n \tag{B.2}$$

$$\dot{Z}_n = 0.006[4(X_n - 1.6) - Z_n], \tag{B.3}$$

where

$$\alpha_n = \sum_{m=1}^{F(U-1)} w_{nm} A_m \tag{B.4}$$

and

$$\beta_n = \frac{1}{F-1} \sum_{m=1}^{F-1} A_m \tag{B.5}$$

are the weighted inter-modular and intra-modular activities, respectively, which are dependent on the synaptic connection weights w_{nm} and the neuronal activity variables A_n. The external input I_n was chosen such that the Hindemarsh-Rose neurons were operating in a chaotic regime.

The network consisted of 128 Hindemarsh-Rose neurons belonging to $U = 16$ different modules with $F = 8$ neurons each. In a learning stage, input memory patterns were stored by updating the synaptic connection weights w_{nm} between different neurons using a Hebbian mechanism based on the activity variables A_n. A neuron was considered active whenever its membrane potential X exceeded the threshold value $\widehat{X} = 0$ and its activity was coded by the variable $A_n = \theta(X_n - \widehat{X})$, where θ is the Heavyside function with $\theta(x) = 1$ if $x \geq 0$ and $\theta(x) = 0$ if $x < 0$. For

these studies we restricted ourselves to 29 time series X_n extracted during the retrieval stage in which the learned connection weights were kept constant. According to their coding properties regarding the retrieval of only two distinguished memory patterns, they belonged to three clusters: 13 of the neurons coded for pattern 1 only, 13 coded for pattern 2 only, and 3 coded for both pattern ("Shared"). The respective time series were labelled by "1", "2" and "S" followed by an index letter. The numerical integration was done using a fourth-order Runge-Kutta integration with a fixed step-size of 0.05 (arbitrary time units). The length of the time series was 32768 data points. The threshold for spike detection was chosen as the arithmetic average over the minimum and maximum value of the respective time series. In Appendix C.1 we follow Kreuz et al. (2007) and evaluate the clustering of all 29 spike trains, whereas in Appendix C.2 we follow Kreuz et al. (2009) and the investigation of the set separations was restricted to the two principal clusters.

Appendix C. Comparison of measures using simulated Hindemarsh-Rose time series

We also evaluate the performance of the newly proposed SPIKE-distances within the bivariate and multivariate setups of the simulated network of Hindemarsh-Rose neurons previously used in Kreuz et al. (2007) and Kreuz et al. (2009), respectively.

C.1. *Bivariate setup: Assessing clustering quality*

One important application for measures of spike train synchrony is the identification of spike train correlations and the recognition of response clusters. In Kreuz et al. (2007) we carried out a controlled comparison of six different spike train distances regarding their capability to reproduce the clustering within a network of 29 Hindemarsh-Rose spike trains (for a description of the data see Appendix B.3).

The measures against which we compared the ISI-distance D_I were the Victor-Purpura distance D_V (Victor and Purpura, 1996), the van Rossum metric D_R (van Rossum, 2001), the inversion of the similarity measure proposed by Schreiber et al. (2003), and the inverted event synchronization D_Q (Quian Quiroga et al., 2002). The van Rossum metric D_R measures the Euclidean distance between the two spike trains after filtering of the spikes with an exponential kernel. The distance D_{Sch} based on the similarity measure proposed by Schreiber et al. (2003) quantifies the normalized cross correlation of spike trains after Gaussian filtering. The inverted event synchronization D_Q (Quian Quiroga et al., 2002) quantifies the number of quasi-simultaneous appearances using a variable time-scale that automatically adapts itself to the local spike rates. Thus D_Q (Quian Quiroga et al., 2002), like the ISI- and the SPIKE-distance, does not need a time-scale parame-
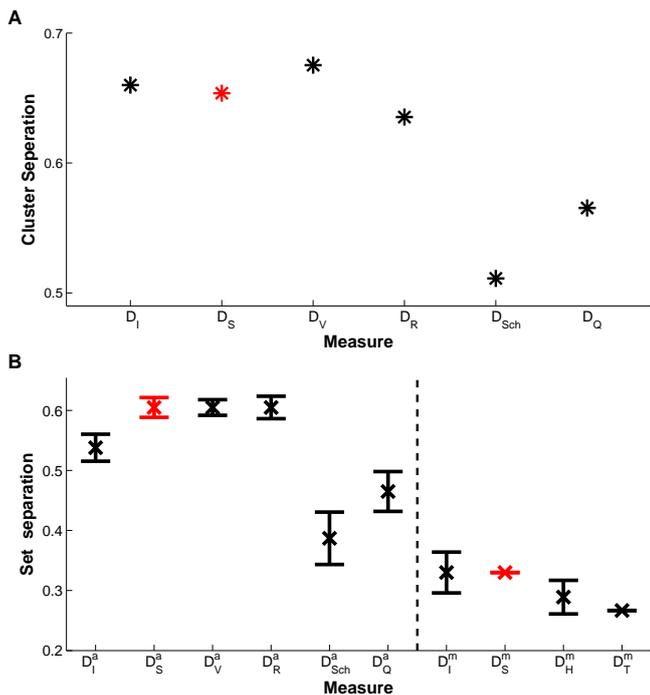
Fig. C.1. (color online) Controlled comparison of spike train distances on a Hindemarsh-Rose network. A. Comparison of bivariate measures: Separation of clusters. B. Comparison of multivariate measures: The set separation is defined as the fraction of tests with a Kolmogorov-Smirnov statistic equal to 1. The dashed line separates the averaged bivariate measures from the multivariate measures. Note that panel A is an extension of Fig. 11 from Kreuz et al. (2007), and panel B is an extension of Fig. 15 from Kreuz et al. (2009).

ter, whereas all other distances rely on a parameter that sets the time-scale of the analysis. These parameters were varied over several orders of magnitude and the highest performance obtained was used to represent the measure.

Details on the analysis can be found in Kreuz et al. (2007). In short: We applied the dissimilarity measures to all possible pairs of spike trains and from the resulting pairwise distance matrices we generated hierarchical cluster trees. From these dendrograms we extracted the cluster separation, an indicator which quantifies how well the different measures can separate the three clusters of the network. We here repeat exactly the same analysis for the spike-based distance D_S. As shown in Fig. C.1A both the ISI- and the SPIKE-distance almost match the cluster separation of the best time-scale optimized measure. The poorest cluster separation is obtained for the optimized D_{Sch}.

C.2. *Multivariate setup: Assessing set separation*

Following Kreuz et al. (2009) we use the same controlled setup with the network of Hindemarsh-Rose neurons to compare the performance of several averaged bivariate and multivariate measures in distinguishing different levels of multi-neuron spike train synchrony. The averaged bivariate measures are the extended variants of the bivariate measures used in Appendix C.1, multivariate measures com-

prise the multivariate ISI- and SPIKE-distances as well as the reliabilities D_H^m by Hunter et al. (1998) and D_T^m by Tiesinga (2004). While D_H^m measures the normalized variance of pooled, exponentially convolved spike trains, D_T^m exploits the deviation of pooled spike train statistics from the one obtained for a Poisson process. Again the performance of the time-scale dependent measures is optimized with respect to the time-scale parameter.

In order to gradually change the level of synchrony in a controlled manner, we construct randomly selected sets of spike trains from the two principal clusters of the Hindemarsh-Rose network and vary the set imbalance, the relative contributions of these clusters. For each set imbalance we create five groups of 100 realizations and then employ the set separation, a simple measure based on Kolmogorov-Smirnov statistics, to quantify how well the distributions of measure values for adjacent set imbalances can be distinguished. We repeat exactly the same analysis for the averaged bivariate SPIKE-distance D_S^a as well as for the multivariate SPIKE-distance D_S^m. Results for all measures are shown in Fig. C.1B.

In this multivariate context the SPIKE-distance matches the performance of the best time-scale optimized measures. The averaged bivariate ISI-distance D_I^a is very close behind. Overall, the averaged bivariate measures are consistently better at distinguishing different set imbalances than the multivariate measures. Among these the highest set separations are obtained for the ISI-distance D_I^m closely followed by the SPIKE-distance D_S^m. This is probably due to the fact that these measures are not invariant to shuffling spikes among the spike trains but rather do take into account the spike train of origin for each individual spike. On the other hand, measures that act on the pooled spike train, such as all measures based on the Peri-Stimulus Time Histogram (PSTH), yield the same value regardless of how spikes are distributed among the different spike trains (cf. also Fig. 3).

References

Abramson N. Information theory and coding. McGraw-Hill, New York, 1963.

Aronov D, Reich DS, Mechler F, Victor JD. Neural coding of spatial phase in V1 of the macaque monkey. J Neurophysiol, 2003;89:3304-27.

Best PJ, White AM, Minai A. Spatial processing in the brain: the activity of hippocampal place cells. Annu Rev Neurosci, 2001;24:459-86.

Chicharro D, Kreuz T, Andrzejak RG. Estimation of information and informative precision of the neural responses from spike train distances discrimination analysis. In preparation.

Chichilnisky EJ. A simple white noise analysis of neuronal light responses. Network: Comput Neural Syst, 2001;12:199-213.

Chichilnisky EJ, Kalmar RS. Functional Asymmetries in ON and OFF Ganglion Cells of Primate Retina. J Neurosci, 2002;22:2737-47.

De Vries SH. Correlated Firing in Rabbit Retinal Ganglion Cells. J Neurophysiol, 1999;81:908-20.

Di Lorenzo PM, Victor JD. Taste Response Variability and Temporal Coding in the Nucleus of the Solitary Tract of the Rat. J Neurophysiol, 2003;90:1418-31.

Field GD, Chichilnisky EJ. Information Processing in the Primate Retina: Circuitry and Coding. Annu Rev Neurosci, 2007;30:1-30.

Field GD, Sher A, Gauthier JL, Greschner M, Shlens J, Litke AM, Chichilnisky EJ. Spatial Properties and Functional Organization of Small Bistratified Ganglion Cells in Primate Retina. J. Neurosci, 2007;27:13261-72.

Gardner D. Neurodatabase.org: networking the microelectrode. Nature Neurosci, 2004;7:486-7.

Hindmarsh JL, Rose RM. A model of neuronal bursting using three coupled first order differential equations. Proc R Soc London B, 1984;221:87-102.

Houghton C, Sen K. A new multineuron spike train metric. Neural Comput, 2008;20:1495-511.

Hunter JD, Milton G, Thomas PJ, Cowan JD. Resonance effect for neural spike time reliability. J Neurophysiol, 1998;80:1427-38.

Kreuz T, Luccioli S, Torcini A. Double coherence resonance in neuron models driven by discrete correlated noise. Phys Rev E, 2006;97:238101.

Kreuz T, Haas JS, Morelli A, Abarbanel HDI, Politi A. Measuring spike train synchrony. J Neurosci Methods, 2007;165:151-61.

Kreuz T, Chicharro D, Andrzejak RG, Haas JS, Abarbanel HDI. Measuring multiple spike train synchrony. J Neurosci Methods, 2009;183:287-99.

Kreuz T, Chicharro D, Andrzejak RG. Measuring spike train synchrony between neuronal populations. In preparation.

Litke AM, Bezayiff N, Chichilnisky EJ, Cunningham W, Dabrowski W, Grillo AA, Grivich M, Grybos, P, Hottowy P, Kachiguine S, Kalmar RS, Mathieson K, Petrusca D, Rahman M, Sher A. What Does the Eye Tell the Brain?: Development of a System for the Large-Scale Recording of Retinal Output Activity. IEEE Trans Nuclear Science, 2004;51:1434-40.

Mastronarde DN. Correlated firing of cat retinal ganglion cells. I. Spontaneously active inputs to X- and Y-cells. J Neurophysiol, 1983;49:303-24.

Meister M, Lagnado L, Baylor DA. Concerted signaling by retinal ganglion cells. Science, 1995;2700:1207-10.

Meister M, Berry MJ. The Neural Code of the Retina. Neuron, 1999;22:435-50.

Morelli A, Grotto RL, Arecchi FT. A feature-based model of semantic memory: The importance of being chaotic. Lecture Notes in Computer Science, 2005;3704:328-37.

Nawrot MP, Aertsen A, Rotter S. Elimination of response latency variability in neuronal spike trains. Biol Cybern, 2003;88:321-34.

Priebe NJ, Ferster D. Inhibition, spike threshold, and stimulus selectivity in primary visual cortex. Neuron, 2008;570:482-97.

Quian Quiroga R, Kreuz T, Grassberger P, 2002. Event synchronization: A simple and fast method to measure synchronicity and time delay patterns. Phys Rev E, 2002;66:041904.

Romo R, Salinas E. Flutter discrimination: neural codes, perception, memory and decision making. Nature Rev Neurosci, 2003;40:203-18.

Schnapf JL, Nunn BJ, Meister M, Baylor DA. Visual transduction in cones of the monkey Macaca fascicularis. J Physiol, 1990;427:681-713.

Schreiber S, Fellous JM, Whitmer JH, Tiesinga PHE, Sejnowski TJ. A new correlation-based measure of spike timing reliability. Neurocomp, 2003;52:925-31.

Schreiner CE, Winer JA. Auditory cortex mapmaking: principles, projections, and plasticity. Neuron, 2007;560:356-65.

Shlens J, Field G, Gauthier JL, Grivich MI, Petrusca D, Sher A, Litke AM, Chichilnisky EJ. The Structure of Multi-Neuron Firing Patterns in Primate Retina. J Neurosci, 2006;26:8254-66.

Shlens J, Rieke F, Chichilnisky EJ. Synchronized firing in the retina. Curr Opin Neurobiol, 2008;18:396-402.

Shlens J, Field GD, Gauthier JL, Greschner M, Sher A, Litke AM, Chichilnisky EJ. The Structure of Large-Scale Synchronized Firing in Primate Retina. J Neurosci, 2009;29:5022-31.

Tiesinga PHE. Chaos-induced modulation of reliability boosts output firing rate in downstream cortical areas. Phys Rev E, 2004;69:031912.

Tiesinga PHE, Fellous JM and Sejnowski TJ. Regulation of spike timing in visual cortical circuits. Nature Rev Neurosci, 2008;9:97-107.

Usrey WM, Reid RC. Synchronous activity in the visual system. Annu Rev Physiol, 1999;61:435-56.

van Rossum MCW. A novel spike distance. Neural Comput, 2001;13:751-63.

Victor JD, Purpura KP. Nature and precision of temporal coding in visual cortex: A metric-space analysis. J Neurophysiol, 1996;76:1310-26.

Victor JD, Purpura KP. Metric-space analysis of spike trains: theory, algorithms and application. Network: Comput Neural Syst, 1997;8:127-64.

Victor JD. Spike train metrics. Curr Op Neurobiol, 2005;15:585-92.

Waddell J, Dzakpasu R, Booth V, Riley B, Reasor J, Poe G, Zochowski M. Causal entropies A measure for determining changes in the temporal organization of neural systems. J Neurosci Methods, 2007;162:320-32.

Wilson RI, Mainen ZF. Early events in olfactory processing. Annu Rev Neurosci, 2006;29:163-201.